Remote Sensing of Environment 163 (2015) 61–69

Contents lists available at ScienceDirect

Remote Sensing of Environment

journal homepage: www.elsevier.com/locate/rse

Spatio-temporal variability of Suomi-NPP VIIRS-derived aerosol optical thickness over China in 2013

Fei Meng [a,b], Changyong Cao [c,*], Xi Shao [b,d]

[a] Department of Civil Engineering, Shandong Jianzhu University, Jinan, P.R. China
[b] Department of Astronomy, University of Maryland, College Park, MD, USA
[c] NOAA/NESDIS/STAR, College Park, MD, USA
[d] Suzhou Demeter Environmental Corporation, Ltd.Changshu, P.R. China

ARTICLE INFO

Article history:
Received 27 August 2014
Received in revised form 1 March 2015
Accepted 3 March 2015
Available online 26 March 2015

Keywords:
Aerosol optical thickness
VIIRS
China
Variability

ABSTRACT

The Visible Infrared Imaging Radiometer Suite (VIIRS) aerosol optical thickness (AOT) at 550 nm Intermediate Product (IP) data was evaluated by comparing it with measurements from Aerosol Robotic Network (AERONET) and Moderate Resolution Imaging Spectroradiometer (MODIS) retrievals. The spatial and temporal variations in the regional AOT over China during 2013 (from 24 January to 31 December) were then firstly investigated using VIIRS aerosol IP data. Evaluation of VIIRS IP AOT with MODIS retrievals and AERONET measurements indicated that the performance of the VIIRS aerosol IP product is comparable to that of their counterparts from the heritage MODIS sensor. However, the VIIRS IP can produce more retrievals than MODIS due to its higher spatial resolution, therefore more suitable for regional AOT study. It was found that the VIIRS IP mean AOT over China differs from that of MODIS by −0.032 for the collocated retrievals, with a correlation of 0.928. Compared with AERONET measurements, VIIRS IP AOT shows a negative bias of −0.058 with the standard deviation of the difference of 0.192 over China. Among the 10 typical sites under study, the maximum annual average AOT550 values (with ± standard deviation) were found in Chengdu (1.07 ± 0.32), whereas the lowest annual mean AOT550 values were found in FB1 (0.242 ± 0.25). The economically developed regions had high AOT values during all seasons. Based on the distribution of AOT, China can be divided into an economically developed eastern region with high AOT values and less-developed western regions, consistent with the boundary between China's second and third terrain regions.

Published by Elsevier Inc.

1. Introduction

Aerosols, which are emitted from various natural or anthropogenic sources, are ubiquitous in the atmosphere of the earth (Zhang, Huang, Zhu, & Rao, 2013). These small suspended solid and liquid particles in the atmosphere, such as smoke, mineral dust, particulate pollution, biogenic compounds and sea salt, play an active role in atmospheric chemistry (Koren et al., 2012) and the Earth's energy balance (Chin, Schwartz, & Kahn, 2009). Studies have shown that these particles with radii below 100 nm can penetrate into the pulmonary alveolus and remain there, causing various diseases when breathed into the lungs (Pope et al., 2002; Van Zelm et al., 2008).

Due to their complicated physical and chemical properties and uneven spatial and temporal distributions, aerosols remain one of the major uncertain factors in estimating climatic forcing (He et al., 2010). Many studies have been conducted on the retrieval of aerosol particle optical properties, their relationship with PM concentrations, their temporal and spatial variations, and their influence on climate systems and atmospheric radiation (Du et al., 2008; Hao, Wang, Li, Hu, & Yu, 2005; He et al., 2010; Lee, Kim, & Han, 2006; Xin et al., 2014; Yang et al., 2014). However, there are still uncertainties due to the poor understanding of aerosol properties and their spatial and temporal variation (Esteve, Estelles, Utrillas, & Martinez-Lozano, 2012; IPCC, 2007). Long-term continuous aerosol observations over large regions are very important in the current assessment and application of public health and global climate (Liu, Zheng, Li, & Wu, 2008).

The most direct way to obtain AOT is from in situ measurements with sun-photometers on the ground. However, there are limited numbers of surface monitoring stations throughout the world due to high operating costs, especially for the remote countryside. Therefore, increasing attention has been given to satellite-based aerosol measurements. As the next-generation polar-orbiting operational environmental sensor with a capability for global aerosol observations, VIIRS aerosol retrieval is expected to continue the decade-long successful aerosol retrieval from MODIS for scientific research and applications (Liu et al., 2014).

Over the past several decades, China has become one of the major factors in the uncertainty of the Earth's aerosol climate due to increases in rapid urbanization and industrial activities (IPCC, 2007; Xin, Wang, Wang, Li, & Wang, 2011). However, the compositions and distributions of aerosols are characterized by a high level of spatial and temporal variability (Chin et al., 2009). The spatial and temporal variations of

* Corresponding author.
E-mail address: changyong.cao@noaa.gov (C. Cao).

http://dx.doi.org/10.1016/j.rse.2015.03.005
0034-4257/Published by Elsevier Inc.

aerosols in China are poorly understood because of the sparse network of observations (Guo et al., 2011). Meng, Cao, Shao, and Shi (2014) investigated the spatial and temporal changes of AOT in Shandong province, China, using aerosol data retrieved from VIIRS. In order to use VIIRS AOT IP product for any quantitative study, first we evaluate its quality with ground measurements (AERONET) over 12 selected sites, and by comparing it to heritage MODIS aerosol data that have already been extensively used in analyzing pollution over China. This is presented in Section 3.2. Once the quality of VIIRS AOT IP data is established to be sufficient, spatial and temporal analysis of the data are performed. This is presented in Section 4.

2. Study area

In the past three decades, China's urban population has rapidly increased from less than 200 million to more than 700 million (NSBC, 2013). Rapid economic growth and population expansion have resulted in drastic increases in energy consumption, which in turn have led to a significant increase of AOT over much of China (Xia et al., 2006). Among the megacities, Shanghai, Beijing, and Guangzhou are the typical, core cities of the Yangtze River Delta (indicated by rectangle "A" in Fig. 1), Bohai Rim (indicated by rectangle "B" in Fig. 1), and the Pearl River Delta (PRD) (indicated by rectangle "C" in Fig. 1), respectively. In addition to large population and economic growth, Chengdu, which is surrounded by high mountains, has a typical geomorphology in the Sichuan basin (indicated by rectangle "D" in Fig. 1). As the traditional heavy industrial base of China (indicated by rectangle "E" in Fig. 1), northeast China suffers from atmospheric pollution created by coal burning mixed with dust from northwestern China (Herman et al., 1997). Studies have also shown that the amount and rates of emission of atmospheric pollutants and primary aerosols were higher in the above regions in the past decade (Guo et al., 2011; Herman et al., 1997; Lee, Kim, Hoyninegen-Huene, & Burrow, 2007). Therefore, the megacities Shanghai, Beijing, Guangzhou, Chengdu, and Shenyang were chosen from the Yangtze River delta, Bohai Rim, Pearl River delta, Sichuan Basin, and northeast China, respectively. Huhehot lies on the Mongolia Plateau and suffers mainly from dust storms especially in the spring. Kunming lies in the Yungui Plateau, where anthropogenic emission is the primary contributor of atmospheric pollution. Two forest sites, FB1 (41.14°N, 117.38°E, 750 m mean elevation) and FB2 (29. 19°N, 109.43°E, 670 m mean elevation), with comparatively lower aerosol loads, were chosen as for the regional background. The sites are located in a hilly area surrounded by forest and are far from any urban areas.

Fig. 1 shows the ten typical Chinese sites under study: Beijing, Shanghai, Guangzhou, Chengdu, Shenyang, Huhehot, Kunming, Aomen, forest background site1 (FB1) and forest background site2 (FB2). To compare the AOT550 in China with neighboring countries, the major cities Hanoi, Vietnam and Muang Xai, Laos, were also studied and are marked in Fig. 1.

3. Data and methods

3.1. VIIRS IP AOT product

VIIRS is one of the key environmental remote sensing instruments onboard the Suomi National Polar-orbiting Partnership (S-NPP) satellite, which was successfully launched on October 28, 2011 from Vandenberg Air Force Base (VAFB), USA. VIIRS is a cross-track scanning radiometer that measures emitted and reflected radiation from the Earth atmosphere system, covering wavelengths from 412 nm to 12,050 nm (Cao, Deluccia, Xiong, Wolfe, & Weng, 2014; Hutchison & Cracknell, 2006). Additionally, VIIRS also features dual gain bands that allow a large dynamic range while retaining a high signal to noise ratio at low radiance values, making the bands useful for both land and atmospheric applications (Cao et al., 2014; Jackson et al., 2013). VIIRS has three types of bands: five imagery bands (I-bands, 375-m resolution at nadir), 16 moderate resolution bands (M-bands, 750-m resolution at nadir), and the day/night band (750-m resolution across scan). The M-bands (M1, M2, M3, M4, M5, M6, M7, M8, M10, and M11) are used to determine aerosol using an aerosol algorithm. Bands M4, M9, M12, M15,

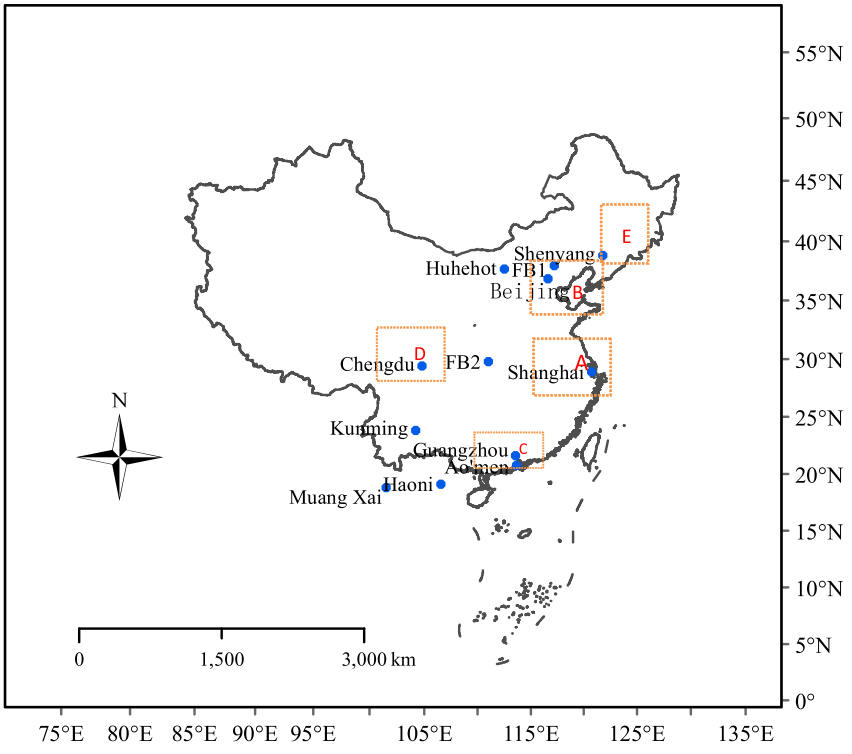

Fig. 1. Location of the study area. A: Yangtze River Delta, B: Bohai Rim, C: Pearl River Delta, D: Sichuan Basin, E: Northeast traditional heavy industrial base of China.

and M16 are used in the internal screening tests for data quality assurance (Jackson et al., 2013).

VIIRS AOT550 retrievals are performed at the M-band pixel level and produce a full series of aerosol parameters called the intermediate product (IP). It is composed of AOT, Ångström exponent, and aerosol model information, including three parameters retrieved over the ocean and a single-aerosol model selected over land. Quality assurance is applied at the IP level with the resulting flags indicating the confidence on the retrievals. For this paper, the screening method for AOT IP was chosen to have the AOT550 Quality Flag = 0 (good), Cloud Quality = 0 (Clear) and to exclude turbid/shallow water. Based on suggestions from other research groups (Ichoku et al., 2002; Remer et al., 2002; Xin et al., 2011), data matching was performed using the following rules: if at least five pixels fell within a 40 km × 40 km box centered on a study site, the mean VIIRS-retrieved AOT550 was calculated. Observed AOT550 with standard deviation > 0.5 was excluded to reduce validation errors (Xin et al., 2011). Then, statistical data were obtained based on the ten typical sites studied.

3.2. Validation data

The spatiotemporal technique proposed in previous studies (Liu et al., 2014; Petrenko, Ichoku, & Leptoukh, 2012) was used to validate the retrieved AOT550 from VIIRS IP against the aerosol optical thickness measurements from AERONET, and the Aqua MODIS Dark Target aerosol product (MYD04) (Levy et al., 2013; Liu et al., 2014). Validation against AERONET and MODIS focused on the period from 24 January to 31 December 2013. The 12 AERONET sites are listed in Table 1.

Data provided by AERONET do not have the 550 nm channel and therefore AOT is calculated by linear interpolation in log scale from two measurements at adjacent wavelengths. To show how well the VIIRS AOT matches the evaluation data sets, the following metrics were calculated as were those of Liu et al. (2014): Pearson correlation coefficient, accuracy (the mean difference between two data sets), precision (the standard deviation of the difference), and uncertainty (the root mean square difference). Additionally, the criteria for a VIIRS-MODIS matchup proposed in previous study are as follows: (1) cloud fraction is zero within the MODIS retrieval domain; (2) the central location of a VIIRS IP retrieval box falls within the MODIS 10 km retrieval domain; and (3) MODIS and VIIRS IP retrievals are within a 5 min time interval (Liu et al., 2014).

For comparison, VIIRS IP/MODIS data (30 km × 30 km) close to each AERONET station were selected. At the same time, AERONET data within ±30 min of VIIRS satellite overpass times were taken. These temporally averaged AERONET AOTs and spatially averaged VIIRS IP/MODIS AOTs were used to validate the VIIRS determined AOT retrieval.

Individual retrieval matchups of VIIRS IP and MODIS AOT550 are shown as scatterplots in Fig. 2, and the statistics are listed in Table 2.

Table 1
Summary of selected AERONET sites used for the validation of satellite products.

Regions	AERONET Site	Lon/Lat	Observing period (MM/DD-MM/DD)	Data
North China	Beijing	116.381/39.977	01/02–10/20	Level 2.0
	Beijing-CAMS	116.317/39.933	01/24–12/31	Level 1.5
	Shijiazhuang	114.550/38.000	12/5–21/31	Level 1.5
	Xianghe	116.962/39.754	01/02–12/31	Level 2.0
	Xuzhou	117.142/34.217	07/09–12/31	Level 2.0
	Baotou	109.629/40.852	09/27–12/12	Level 2.0
	Taihu	120.215/31.421	01/02–12/31	Level 1.5
	Hong Kong PolyU	114.180/22.303	01/05–06/07	Level 2.0
South China	Hong Kong Sheung	114.117/22.483	01/02–07/11	Level 2.0
	Taiwan-Chiayi	120.496/23.496	09/26–12/31	Level 2.0
	Heng-Chun	120.700/22.055	03/29–05/27	Level 2.0
	Lulin	120.874/23.469	01/12–03/17	Level 2.0

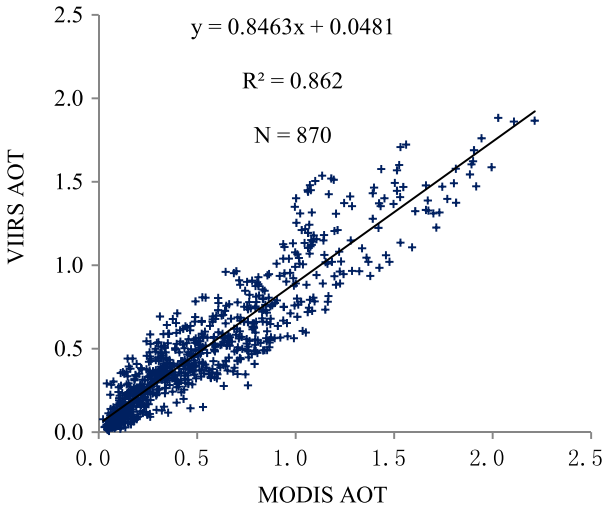

Fig. 2. Scatterplots between collocated VIIRS IP AOT550 and MODIS AOT550.

The number of retrievals from VIIRS IP and MODIS are 2689 and 934 respectively with good consistency, indicating more retrievals from VIIRS IP. It is noted that MODIS spatial resolution becomes lower at high scan angles off nadir (from 1 km to several kilometers), whereas VIIRS IP has better spatial resolution with low pixel size growth across its scan (from 0.75 km to 1.6 km) (Cao et al., 2014). Note that the number of matchups is 870, which were used in the analysis and limited to collocations in which VIIRS IP and MODIS retrievals occurred at the same sites and dates. As seen from Table 2, the overall good agreement between VIIRS IP and MODIS AOT550 retrieval is demonstrated by the standard deviation (0.113) and high correlation (0.928).

A comparison of individual retrieval matchups of VIIRS IP and AERONET AOT550 are displayed as scatterplots in Fig. 3, and the statistics are listed in Table 3. The VIIRS IP derived AOT550 were found to be in good agreement with the AERONET sun photometer-derived AOT550 with a high correlation (0.907), accuracy (−0.058), and precision (0.192) for all sites. Generally, the line along the Huai River-Qinling Mountains acts as the north–south boundary of climate. To demonstrate the regional differences in VIIRS IP, scatterplots of VIIRS IP AOT550 against AERONET AOT550 over sites from south China (Taihu, Hong Kong and Taiwan) and north China (Beijing, Shijiazhuang, Xianghe and Xuzhou) were further analyzed (Fig. 3(b) and (c)). The Validation statistics show that both sites from north China and south China are in good agreement with AERONET with similar correlations (0.887 versus 0.841), but sites from north China exhibits a higher standard deviation in AOT as shown in precision 0.194 verse 0.172) and uncertainty (0.195 verse 0.174).

Time series of the daily mean AOT550 derived from VIIRS IP retrieval against MODIS and AERONET were also studied (Fig. 4). As seen from Fig. 4(a), the temporal variation of VIIRS IP AOT550 was consistent with the MODIS retrievals, and the difference between the two data sets (VIIRS IP-MODIS) of the mean daily AOT550 is −0.032. While Fig. 4(b) indicates that AOT550 from VIIRS IP and AERONET appears to be temporally stable and consistent with each other; the difference between the two data sets (VIIRS IP-AERONET) of the mean daily AOT550 is −0.060 over Beijing.

To further investigate the temporal variation of retrieval difference on a regional basis, the time series of VIIRS IP and MODIS aerosol retrieval errors for north and south China (Table 1) are shown in Fig. 5(a) and (b). Note that the matchups (VIIRS IP – AERONET, MODIS – AERONET) were not exactly at the same times and locations, and the number of daily matchups for both regions was limited. Sometimes a single match was used to represent the daily mean for the entire region, leading to high fluctuations in the time series. Over north China, VIIRS IP tended to overestimate from May to early October but underestimated from January to

Table 2
Statistics of the comparison between collocated VIIRS and MODIS AOT550 [a].

Item	VIIRS	MODIS	VIIRS-MODIS
Mean AOT550	0.492	0.524	−0.032
Standard deviation	0.387	0.425	0.113
Number of matchups		870	
Retrieval counts	2689	934	
Correlation		0.928	

[a] Matchups used in this analysis are limited to collocations in which VIIRS and MODIS retrievals occur at same sites and date.

Table 3
Statistics of the comparison between VIIRS derived AOT550 and AERONET measurements.

Item	Sites from North China	Sites from South China	All sites
Sample size	327	113	440
Accuracy	−0.061	−0.067	−0.058
Precision	0.194	0.172	0.192
Uncertainty	0.195	0.174	0.194
Correlation	0.887	0.832	0.907

April and October to December. VIIRS IP also tended to overestimate over south China from the end of March to late October. MODIS had the same trend as VIIRS IP both in north China and south China, but appeared to have a larger positive bias than VIIRS IP. Additionally, VIIRS IP tended to underestimate when the AOT550 value was high (e.g., when AOT550 higher than 1.8).

4. Results and discussion

4.1. Annual and seasonal AOT550 variations for different cities

The statistical annual VIIRS IP AOT data over 10 sites in China are given in Table 4. The values of annual average AOT550 were sequenced from high to low from Chengdu (1.07), Guangzhou (1.01), Shanghai (0.86), Beijing (0.67), Aomen (0.65), Shenyang (0.62), Kunming (0.52), Huhehot (0.44), FB2 (0.46) and FB1 (0.27). While the annual mean AOT550 values of Hanoi, Vietnam and Muang Xai, Laos were respectively 0.92 and 0.48 (Fig. 1).

Comparatively, the annual mean VIIRS AOTs in Table 4 are very similar to those from other studies that used longer record. As the most densely populated and industrialized cities in China, the megacities Chengdu, Guangzhou, Shanghai, and Beijing had significantly higher AOT550 values. Which have also been reported in previously studies (Luo, Zheng, Zhao, & Chen, 2014; Qu et al., 2010). The highest annual mean AOT550 was found in Chengdu (0.848) by Luo et al. (2014) using 10-year (March 2000 to February 2010) MODIS data. Xin et al. (2011) found that the annual averaged AOT550 in the forest (39.97°N, 115.43°E) nearby FB1 was 0.20 from 2004 to 2010.

4.2. Spatiotemporal pattern of AOT550

Statistical analysis was performed to study the spatial and temporal variations of the regional AOT550. As shown in Table 4, the megacities Chengdu, Guangzhou, Shanghai, and Beijing had significantly higher

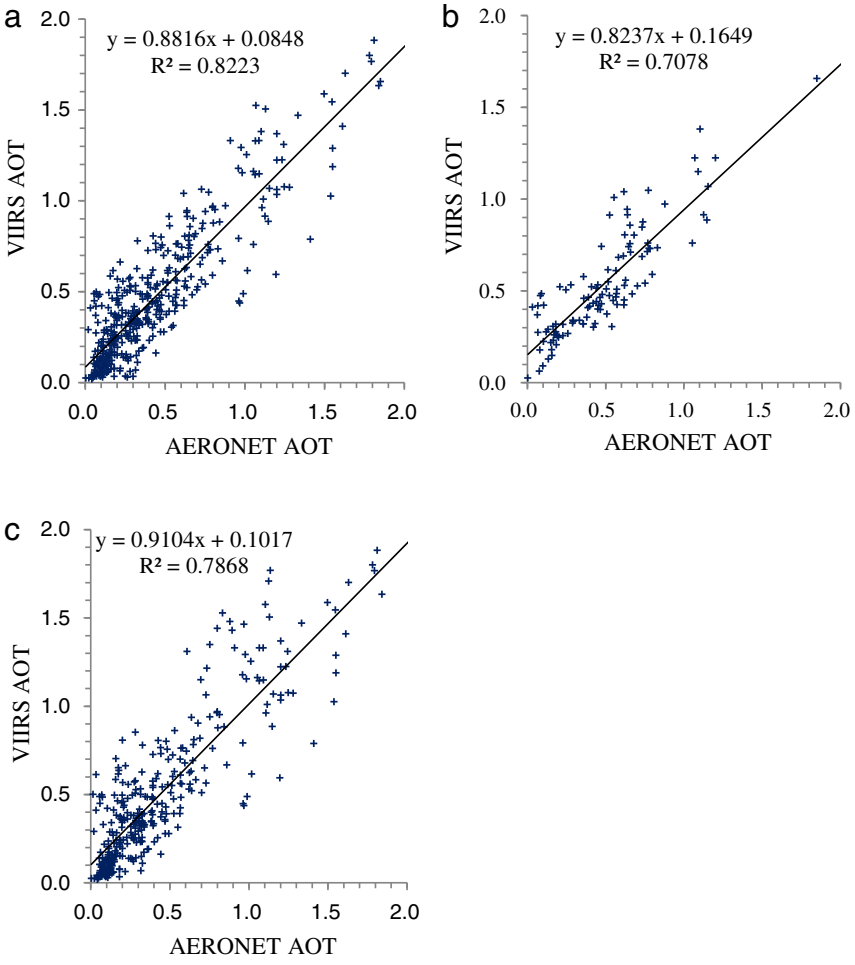

Fig. 3. Scatterplots of VIIRS IP AOT550 against AERONET sun photometer-derived AOT550 over (a) all 12 sites over China, (b) sites from South China (Taihu, Hong Kong and Taiwan), (c) sites from North China (Beijing, Shijiazhuang, Xianghe and Xuzhou).

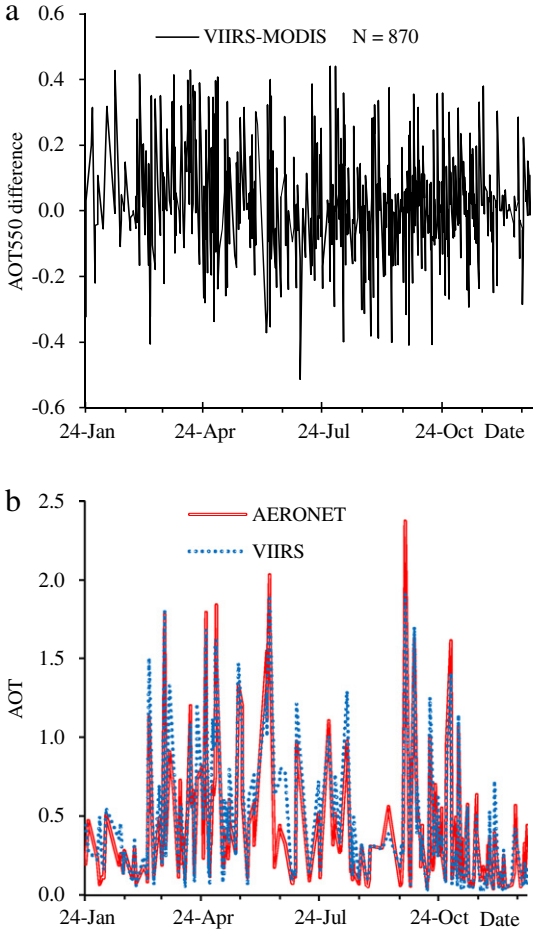

Fig. 4. Time series of the daily mean AOT550 derived from VIIRS IP: (a) against MODIS over China; (b) temporal variation with the AERONET over Beijing.

AOT550 values. Furthermore, they are the typical core cities of the Sichuan Basin, PRD, Yangtze River Delta, and Bohai Rim, respectively. Therefore, the above four cities and two regional forest background sites FB1 and FB2 were further studied. Seasonal and monthly averaged AOT550, weighted by the number of pixels over each site during a given month or season from cloud-free pixels, were calculated.

Table 4
Statistical annual AOT data for cities in China.

City	N	Min.	Max.	Mean	STD	Variance
Huhehot	152	0.02	1.20	0.44	0.24	0.06
Kunming	228	0.04	1.18	0.52	0.29	0.09
Shenyang	183	0.05	1.47	0.62	0.37	0.14
Aomen	151	0.30	1.38	0.65	0.28	0.08
Beijing	214	0.05	1.80	0.67	0.44	0.22
shanghai	212	0.26	1.73	0.86	0.32	0.10
Guangzhou	180	0.31	1.56	1.01	0.33	0.11
Chengdu	151	0.31	1.65	1.07	0.32	0.10
FB1 site	253	0.01	1.45	0.27	0.29	0.10
FB2 site	164	0.10	1.34	0.46	0.26	0.07
Muang Xai	122	0.04	1.30	0.48	0.32	0.11
Hanoi	140	0.25	1.73	0.92	0.36	0.13

The variances of the monthly mean AOT550 values of the above four typical cities and forest background sites were calculated. As shown in Fig. 6, Guangzhou and Chengdu showed comparatively steady and larger AOT550 values all year long, mainly from 0.64 in December to 1.30 in May for Guangzhou and 0.82 in January to 1.22 in August for Chengdu, whereas Shanghai and Beijing showed low AOT550 values in January and then increased quickly to 1.17 in June. Using thirty-three months (2001–2004) of aerosol data in Beijing, Xia et al. (2006) found that the AOT at 440 nm increased from January (0.41) to June (1.25) and then decreased gradually. In this paper, the monthly mean AOT550 values in Hanoi also showed the same trend as that of Guangzhou. Climatologically, all four cities are located in the East Asian monsoon area. Usually, the northward advances of the summer monsoon govern the shifts of precipitation belts with the pre-summer rainy period in the Pearl River Delta from late April to early June and the Meiyu period in the Yangtze River Delta during mid-June and late July (Ding, 1994; Luo et al., 2014). The low AOT550 between May and June corresponded to the pre-summer rainy period in Guangzhou (Fig. 6); The Meiyu rainfall in Shanghai also corresponded to one low AOT550 during the rainy period from June to July (Fig. 6). Furthermore, the North China Plain is also in the monsoon regions, where rainfall occurs usually from late July to early September. With the late monsoon precipitation washout, the AOT550 peak of Beijing was observed in June. 1994). Additionally, there were two peaks and one low in the monthly AOT550 variations of Chengdu between March and August, which were also reported in a previous study (Luo et al., 2014); these were caused by aerosol washout by the monsoon rainfalls and their evolution.

The annual averaged AOT550 values (±standard deviation) in FB1 and FB2 are 0.270 ± 0.286 and 0.468 ± 0.264, respectively, which

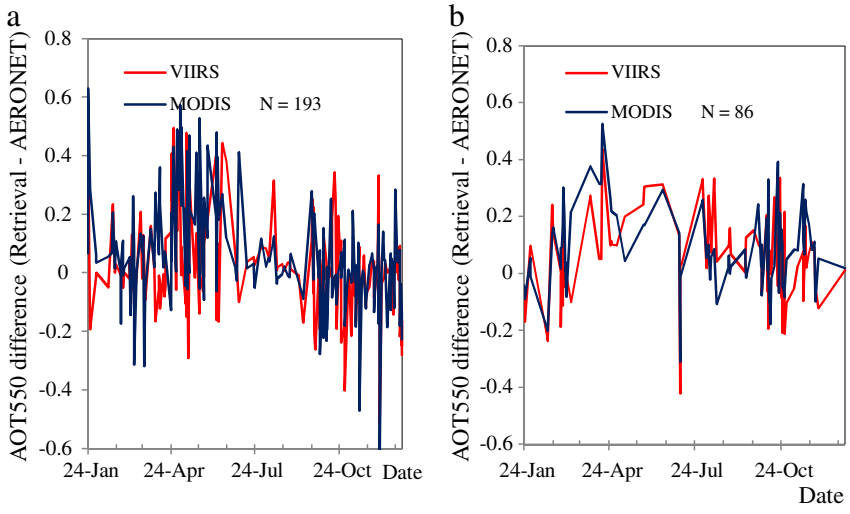

Fig. 5. Time series of the daily mean AOT550 derived from VIIRS IP (or MODIS) against AERONET measurements from 24 January to 31 December 2013, (a) North China; (b)South China; N: the number of matchups.

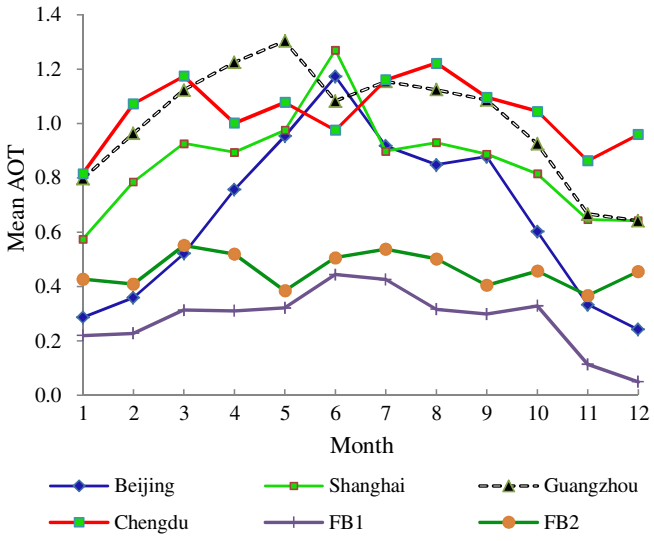

Fig. 6. Monthly averaged VIIRS IP AOT550 over four typical cities and forest background sites.

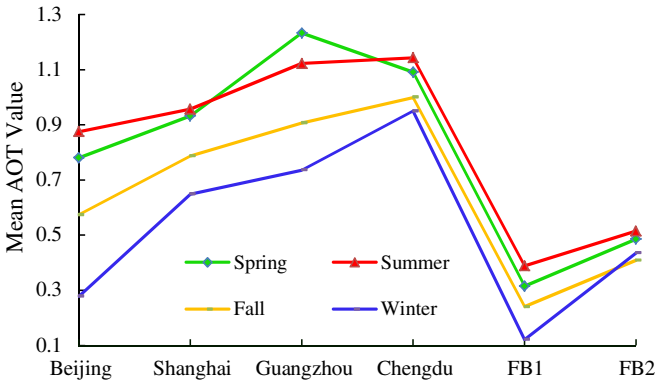

Fig. 7. Statistical seasonal overview of the mean AOT550 in four cities and FB1 and FB2.

were much higher than the background of the North American continental AOT level of 0.10 at 500 nm but lower than AOT550 values nearby cities (Holben et al., 2001). Soil erosion and dust storms are common during the transition from spring to summer, and studies show that the dominant aerosol types are soil and dust aerosols, especially in northern China (Du et al., 2008; Xin et al., 2011). The lowest mean aerosol was found in FB1 with AOT550 values decreased to ~0.10 from November to December. Fossil fuel generates more soot aerosols in the fall and winter. At the same time, a gradual increase in ice and snow cover on the land surface restricts the emission of mineral particles in the winter season (Cao, Zhang, Wang, & Zheng, 2005; Yan, Ohara, & Akimoto, 2006). There are increases in June and October both for FB1 and FB2 (Fig. 6), which may be due to straw burning in June and October. Holben et al. (2001) studied the monthly averaged aerosol optical depth at 500 nm for the period of 1993–1999 at the Goddard Space Flight Center (39°01′N, 76°52′W) located in Washington-Baltimore region (where the author has visited for a year). They found that the aerosol optical depth reached peaks during July and August, with the seven-year July mean of 0.48. However, it decreases to a minimum during winter months, averaging ~0.10 from November to January.

The statistical seasonal overview of the mean AOT550 in four cities and FB1 and FB2 is shown in Fig. 7. The seasonal cycles of VIIRS IP derived AOT showed a maximum in summer (except for Guangzhou) and a minimum in winter and fall. But the mean AOT550 value in the summertime is similar to that in the springtime. The results are consistent with the findings of the existing literature (Kim, Yoon, Kim, & Kim, 2007; Lee et al., 2007). Based on MODIS derived AOT data of 2004, Lee et al. (2007) found a maximum value 0.75 ± 0.18 in summer and 0.49 ± 0.03 in winter over East China. While Kim et al. (2007) found a maximum in spring and a minimum in fall and winter over East Asia using multi-year columnar aerosol property data from MODIS, and AERONET Sun/sky radiometer.

To evaluate the spatial distribution of the seasonal variation, seasonally averaged AOT550 weighted by the number of pixels in an area of $0.02° \times 0.02°$were calculated. Due to snow, cloud, or other bright surfaces, there were some pixels with no data in the composite maps (white regions). As can be seen from Fig. 8, high AOT centers were situated in the most populated and developed regions, including North China Plain, Yangtze River Delta, Pearl River Delta, Sichuan Basin. Although the intensities vary from season to season, the spatial AOT patterns do not change. In addition to the high AOT centers noted above with high anthropogenic aerosols, Luo et al. (2014) found another high AOT center dominated with desert dust that situated in Trim Basin in Northwest China. As seen from Fig. 8, higher seasonal mean AOT550 values were related to the distribution of urban areas. The aerosols for Shanghai, Beijing, Guangzhou, and Chengdu have significantly higher annual mean AOT550 values that may result from intense anthropogenic sources. As Xin et al. (2011) estimated, the anthropogenic emissions and the generation of additional aerosols in the summer accounted for 58% of the aerosol load in Beijing City. The western part of China is generally more influenced by natural sources, such as dust storms, whereas eastern China more affected by anthropogenic activities. As shown in Fig. 8(e), China can be divided into the economically developed eastern region with high AOT550 values and the less-developed western regions along the Great Khingan, Taihang, Wushan, and Xuefeng Mountains based on the distribution of AOT550 (the red dashed line in Fig. 8(e)). Yao and Lu (2014) suggested that the distribution of PM2.5 concentration is consistent with China's three gradient terrains, where the red dash line in Fig. 8(e) is almost the same as the boundary between the second and third gradient terrains. The population, climate, geography, and economy are closely related to the distribution of aerosol optical thickness over China.

As seen from Fig. 1, Beijing is near forest background FB1, Guangzhou is close to the coastal city Aomen, and Chengdu is near FB2. To investigate the temporal change of the daily AOT550 in China, the time series plots of daily AOT550 and the seven-day moving average line of Beijing & FB1, Guangzhou & Aomen, and Chengdu & FB2 in 2013 are illustrated in Fig. 9. The AOT values of Beijing are higher but consistent with FB1, and the same trend can be found with Chengdu & FB2. As reported by the Beijing Environmental Bulletin (2005), the PM10 concentration in the northern suburban areas was approximately 30% lower than that of urban areas. The high background concentrations suggest the importance of regional sources of PM10 in Beijing. Major haze events can be found in Fig. 9(a), such as on May 5–7, July 12–14, and October 3–5. The differences between Aomen and Guangzhou perhaps show that coastal cities have lower AOT550 values than inland cities.

5. Conclusions

The VIIRS IP AOT550 was first evaluated by comparing it with measurements from AERONET and Aqua MODIS (MYD04) retrievals. The validation results show that the performance of VIIRS IP AOT550 is comparable to that of Aqua MODIS over China. The overall good agreement between collocated VIIRS IP and MODIS AOT550 retrievals is demonstrated with standard deviation difference (0.113) and high correlation (0.928). Additionally, the temporal variation of the VIIRS IP AOT550 was also consistent with the MODIS retrievals, and the mean difference between the two data sets (VIIRS IP-MODIS) is −0.032. Compared with AERONET measurements, both sites from north and south China were in good agreement with AERONET and had similar correlations (0.887 versus 0.841), but sites from north China exhibits a higher

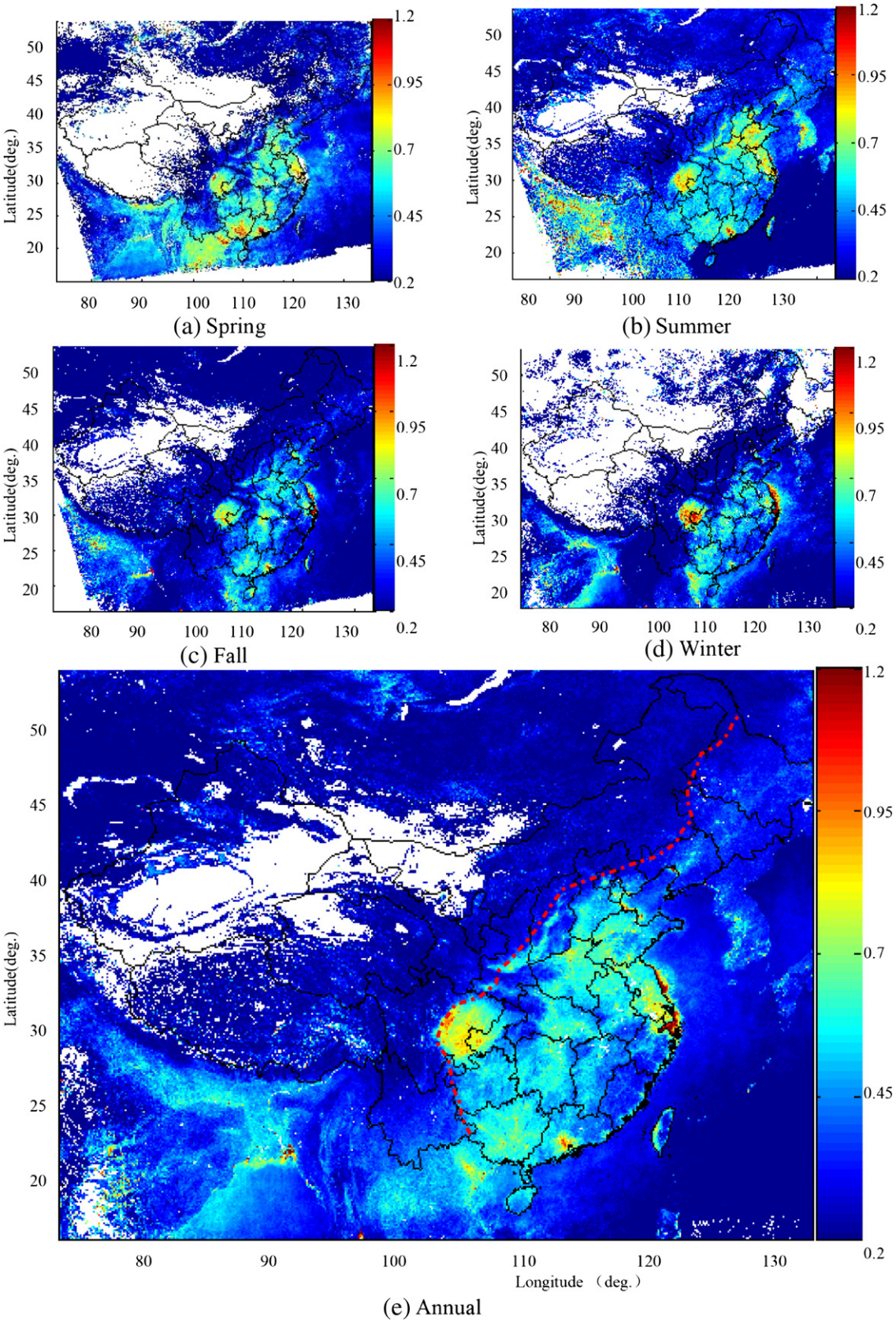

Fig. 8. Seasonal and annual mean AOT550 over China in 2013, white: no data; dashed line: the line divides high and low AOT550 values.

standard deviation as shown in precision (0.194 verse 0.172). Validation against AERONET measurements also showed that VIIRS tended to overestimate in warm months and underestimate during the cold moths.

High AOT centers were situated in the most populated and developed regions, including North China Plain, Yangtze River Delta, Pearl River Delta, and Sichuan Basin. Although the intensities vary from

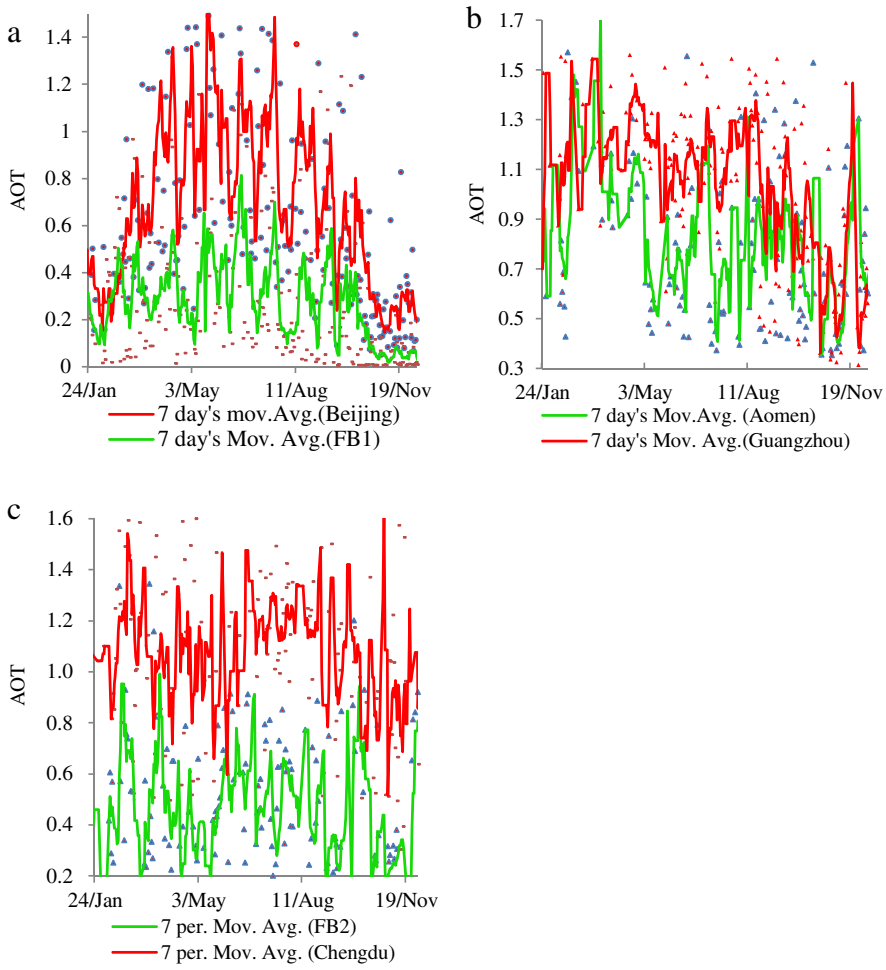

Fig. 9. Time series plots of the daily AOT550 (symbols) and seven-day moving average line (solid lines) in 2013. (a) Beijing & FB1, (b) Guangzhou & Aomen, (c) Chengdu & FB2.

season to season, the spatial AOT patterns do not change. The distribution of AOT550 is consistent with the boundary between the second and third China's gradient terrains. The population, climate, geography, and economy are closely related to the distribution of aerosol optical thickness over China. Further investigation is needed to validate the aerosol type with additional in situ ground measurements.

Acknowledgements

This work was funded by the National Natural Science Foundation of China [41271413] and the Chinese National Key Project [41130525]. We would like to thank the VIIRS and MODIS teams and AEONET principal investigators. Finally, we would like to thank the anonymous reviewers for their constructive comments.

References

Cao, C., Deluccia, F., Xiong, X., Wolfe, R., & Weng, F. (2014). Early On-orbit Performance of the Visible Infrared Imaging Radiometer Suite (VIIRS) onboard the Suomi National Polar-orbiting Partnership (Suomi-NPP) Satellite. *IEEE Transactions on Geoscience and Remote Sensing, 2*, 1142–1156.

Cao, G., Zhang, X., Wang, D., & Zheng, F. (2005). Inventory of atmospheric pollutants discharged from biomass burning in China continent. *China Environmental Science, 25*(4), 389–393 (in Chinese).

Chin, M., Schwartz, S. E., & Kahn, R. A. (2009). *Atmospheric aerosol properties and climate impacts.* Washington, D C, USA: U.S. Climate Change Science Program, 115.

Ding, Y. H. (1994). *Monsoons over China.* Dordercht/Boston, London: Kluwer Academic Publishers.

Du, W., Xin, J., Wang, M., Gao, Q., Li, Z., & Wang, Y. (2008). Photometric measurements of spring aerosol optical properties in dust and non-dust periods in China. *Atmospheric Environment, 42*, 7981–7987.

Esteve, A. R., Estelles, V., Utrillas, M. P., & Martinez-Lozano, J. A. (2012). In-situ integrating nephelometer measurements of the scattering properties of atmospheric aerosols at an urban coastal site in western Mediterranean. *Atmospheric Environment, 47*, 43–50.

Guo, J. P., Zhang, X. Y., Wu, Y. R., Zhaxi, Y. Z., Che, H. Z., & La, B. (2011). Spatial-temporal variation trends of satellite-based aerosol optical depth in China during 1980–2008. *Atmospheric Environment, 45*, 6802–6811.

Hao, J., Wang, L., Li, L., Hu, J. N., & Yu, X. C. (2005). Air pollutants contribution and control strategies of energy-use related sources in Beijing. *Science in China, Series D, 48*(Suppl. II), 138–146.

He, Q. S., Li, C. C., Tang, X., Li, H. L., Geng, F. H., & Wu, Y. L. (2010). Validation of MODIS derived aerosol optical depth over the Yangtze River Delta in China. *Remote Sensing of Environment, 114*, 1649–1661.

Herman, J. R., Bhartia, P. K., Torres, O., Hsu, C., Seftor, C., & Celarier, E. (1997). Global distribution of UV-absorbing aerosols from Nimbus 7/TOMS data. *Journal of Geophysical Research, 102*, 16911–16922.

Holben, B. N., Tanré, D., Smirnov, A., Eck, T. F., Slutsker, I., Abuhassan, N., et al. (2001). An emerging ground based aerosol climatology: aerosol optical depth from AERONET. *Journal of Geophysical Research, 106*, 12067–12097.

Hutchison, K. D., & Cracknell, A. P. (2006). *Visible infrared imager radiometer suite: a New operational cloud imager.* Baton Roca: CRC/Taylor & Francis.

Ichoku, C., Chu, D. A., Mattoo, S., Kaufman, Y. J., Remer, L. A., Tanré, D., et al. (2002). A spatio-temporal approach for global validation and analysis of MODIS aerosol products. *Geophysical Research Letters, 29*, 8006–8010.

Intergovernmental Panel on Climate Change (IPCC) (2007). *Climate change 2007: the physical science basis.* New York: Cambridge University Press, 131–216.

Jackson, J. M., Liu, H., Laszlo, I., Kondragunta, S., Remer, L. A., Huang, J., et al. (2013). Suomi-NPP VIIRS aerosol algorithms and data products. *Journal of Geophysical Research, [Atmospheres], 118*, 12673–12689.

Kim, S. W., Yoon, S. C., Kim, J., & Kim, S. Y. (2007). Seasonal and monthly variations of columnar aerosol optical properties over east Asia determined from multi-year MODIS, LIDAR, and AERONET Sun/sky radiometer measurements. *Atmospheric Environment, 41*, 1634–1651.

Koren, I., Altaratz, O., Remer, L. A., Feingold, G., Martins, J. V., & Heiblum, R. (2012). Aerosol-induced intensification of rain from the tropics to the midlatitudes. *Nature Geoscience, 5*, 118–122.

Lee, K. H., Kim, Y. J., & Han, J. S. (2006). Characteristics of aerosol observed during two severe haze events over Korea in June and October 2004. *Atmospheric Environment*, *40*, 5146–5155.

Lee, K. H., Kim, Y. J., Hoyninegen-Huene, W. V., & Burrow, J. P. (2007). Spatial-temporal variability of satellite-derived aerosol optical thickness over Northeast Asia in 2004. *Atmospheric Environment*, *41*, 3959–3973.

Levy, R. C., Mattoo, S., Munchak, L. A., Remer, L. A., Sayer, A. M., & Hsu, N. C. (2013). The Collection 6 MODIS aerosol products over land and ocean. *Atmospheric Measurement Techniques Discussions*, *6*, 159–259.

Liu, H. Q., Remer, L. A., Huang, J. F., Huang, H. C., Kondragunta, S., Laszlo, I., et al. (2014). Preliminary evaluation of S-NPP VIIRS aerosol optical thickness. *Journal of Geophysical Research – Atmospheres*, *119*(7), 3942–3962.

Liu, J. J., Zheng, Y. F., Li, Z. Q., & Wu, R. J. (2008). Ground-based remote sensing of aerosol optical properties in one city in Northwest China. *Atmospheric Research*, *89*, 194–205.

Luo, Y. X., Zheng, X. B., Zhao, T. L., & Chen, J. (2014). A climatology of aerosol optical depth over China from recent 10 years of MODIS remote sensing data. *International Journal of Climatology*, *34*(3), 863–870.

Meng, F., Cao, C. Y., Shao, X., & Shi, Y. G. (2014). Spatial and temporal variation of Visible Infrared Imaging Radiometer Suite (VIIRS)-derived aerosol optical thickness over Shandong, China. *International Journal of Remote Sensing*. http://dx.doi.org/10.1080/01431161.2014.939784.

National Statistical Bureau of China (2013). *China Statistics Yearbook 2013*. Beijing: National Statistical Bureau of China press.

Petrenko, M., Ichoku, C., & Leptoukh, G. (2012). Multi-sensor aerosol products sampling system (MAPSS). *Atmospheric Measurement Techniques*, *5*, 913–926.

Pope, C. A., III, Burnett, R. T., Thun, M. J., Calle, E. E., Krewski, D., Ito, K., et al. (2002). Lung cancer, cardiopulmonary mortality, and long-term exposure to fine particulate air pollution. *Jama-journal of the American Medical Association*, *287*, 1132–1141.

Qu, W. J., Arimoto, R., Zhang, X. Y., Zhao, C. H., Wang, Y. Q., Sheng, L. F., et al. (2010). Spatial distribution and interannual variation of surface PM10 concentrations over eighty-six Chinese cities. *Atmospheric Chemistry and Physics*, *10*, 5641–5662.

Remer, L. A., Tanre, D., Kaufman, Y. J., Ichoku, C., Mattoo, S., Levy, R., et al. (2002). Validation of MODIS aerosol retrieval over ocean. *Geophysical Research Letters*, *29*, 1618–1621.

Van Zelm, R., Huijbregts, M. A. J., den Hollander, H. A., van Jaarsveld, H. A., Sauter, F. J., Struijs, J., et al. (2008). European characterization factors for human health damage of PM10 and ozone in life cycle impact assessment. *Atmospheric Environment*, *42*, 441–453.

Xia, X. A., Chen, H. B., Wang, P. C., Zhang, W. X., Goloub, P., Chatenet, B., et al. (2006). Variation of column-integrated aerosol properties in a Chinese urban region. *Journal of Geophysical Research*, D06204. http://dx.doi.org/10.1029/2005JD006203 (2006a).

Xin, J. Y., Wang, L. L., Wang, Y. S., Li, Z. Q., & Wang, P. C. (2011). Trends in aerosol optical properties over the Bohai Rim in Northeast China from 2004 to 2010. *Atmospheric Environment*, *45*, 6317–6325.

Xin, J. Y., Zhang, Q., Wang, L. L., Gong, C. S., Wang, Y. S., Liu, Z. R., et al. (2014). The empirical relationship between the PM2.5 concentration and aerosol optical depth over the background of North China from 2009 to 2011. *Atmospheric Research*, *138*, 179–188.

Yan, X., Ohara, T., & Akimoto, H. (2006). Bottom-up estimate of biomass burning in mainland China. *Atmospheric Environment*, *40*, 5262–5273.

Yang, L. K., Xue, Y., Guang, J., Kazemian, H., Zhang, J. H., & Li, C. (2014). Improved aerosol optical depth and Ångstrom exponent retrieval over land from MODIS Based on the Non-Lambertian forward model. *IEEE Geoscience and Remote Sensing Letters*, *11*, 1629–1633.

Yao, L., & Lu, N. (2014). Spatiotemporal distribution and short-term trends of particulate matter concentration over China, 2006–2010. *Environmental Science and Pollution Research International*, *21*, 9665–9675.

Zhang, X. L., Huang, Y. B., Zhu, W. Y., & Rao, R. Z. (2013). Aerosol characteristics during summer haze episodes from different source regions over the coast city of North China Plain. *Journal of Quantitative Spectroscopy & Radiative Transfer*, *122*, 180–193.